《原　著》

SCINTI-PHOTO RESOLUTION AND EVALUATION OF SCINTILLATION CAMERA SYSTEM

Kenji ISHIMATSU*, Ken UEDA**, Masatoshi TANAKA*, and Nobuyuki MUKAI*

ABSTRACT Spatial resolution of scintigram is affected by the performance of scintillation camera system, conditions for imaging and parameters of object, and is represented by critically resolvable distance between two adjacent bars in a scinti-photo of bar phantom by human eyes.

The scinti-photo resolution thus defined is theoretically related with the performance of scintillation camera system and conditions for imaging: i.e. resolution and sensitivity of scintillation camera itself, activity level of radioisotope and imaging time with given parameters of object.

This relation is applied to the evaluation of scintillation camera system.

Firstly, the optimum collimator for a given scintillation camera can be determined when activity level and imaging time are given, and secondly, a definite evaluation of scintillation camera can be made in relation to its resolution and sensitivity, Finally, both experimental and theoretical evaluations were carried out with four commercially available scintillation camera systems.

The experimental resuts are in a good agreement with the theoretical ones, and they indicate that a thinner scintillation crystal does not always result in poorer system performance.

The spatial resolution of a scintillation camera system is determined by the spatial resolution of the scintillation camera and parallel-hole collimator. Collimator sensitivity (i.e. geometrical efficiency), however, depends closely on collimator resolution. Therefore, when system performance is considered, an expression which includes system spatial resolution and sensitivity is required. Coltman[1] and Iinuma et al.[2] investigated the critical limit of human eyes for detecting defects in a scintigram originally including Poisson noise. Rollo et al.[3,4] proposed an index which includes system spatial resolution and sensitivity. The index represents how well a system reproduces in a scintigram an object having a specific geometry for a given exposure time. Keller and Coltman[5] made theoretical considerations on the scintigram resolution in terms of system resolution and sensitivity.

* Hitachi Medical Corporation, Tokyo
** Hitachi Central Research Laboratory, Hitachi Ltd., Tokyo
受付：53年4月3日
最終稿受付：53年11月22日
別刷請求先：国分寺市東恋ケ窪1-280 (〒185)
株式会社日立製作所中央研究所
植　田　　健

On the other hand, scinti-photos are one of the most important outputs of the system, because scinti-photos are usually utilized for diagnostic purposes without any modification. Then, if a system can be evaluated quantitatively by means of obtained scinti-photos, the evaluation method is practical.

In this report, scinti-photo resolution, defined as the resolution of scinti-photos, is discussed theoretically in terms of resolution and sensitivity of the system used. The results are applied to evaluate systems, ans some of them are compared with the experimental results.

Scinti-photo Resolution Versus Average Information Density

At the critical limit of human eyes for detecting defects in a uniform background including Poisson noise, the following semiempirical formula holds, independent of defect size[2]:

$$\sqrt{B}/p = 1 \qquad (1)$$

where B is the average count per "pixel" in the background, and p the depth of a defect (Fig.1.A). This equation is assumed adaptable for scinti-photos of bar phantoms. In this case (Fig. 1.B), B is the average count per pixel in the hottest region

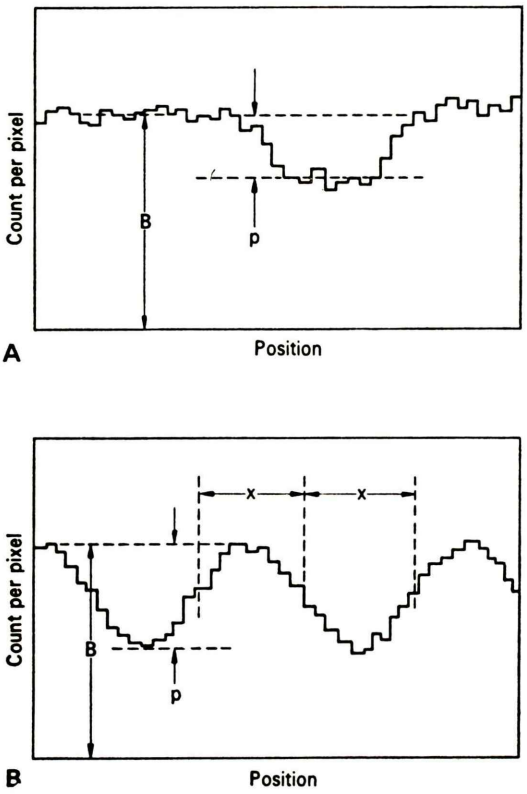

Fig. 1 One dimensional models of images including Poisson noise: (A) defect in uniform background, and (B) bar phantom.

of the image, and p the difference between the counts in the hottest and coldest regions. That is:

$$B = n_{av} \cdot S_e \cdot (0.5+d)/0.5 \qquad (2)$$

$$p = 2 \cdot n_{av} \cdot S_e \cdot 2d \qquad (3)$$

where n_{av} is the average information density (i.e. the average count per unit area in the detector surface), and S_e is the area of a virtual pixel, $2d$ is defined as the ratio of difference in count per pixel between the hottest and coldest regions to average count per pixel.

Here, S_e is assumed to be expressed as:

$$S_e = k \cdot x^2 \qquad (4)$$

where x is the distance between two adjacent bars of the phantom, or the bar width, and k is a constant. This assumption is based on that there exsists an optimum distance between the human eye and a bar phantom image. This optimum distance, d_o, is assumed to be proportional to $m_i\, x$, the product of the bar width and magnification factor of the image, m_i. The area of virtual pixel, the resolvable area by human eyes, is proportional to d_o^2/m_i^2. Then, S_e is proportional to x^2.
The conbination of eqs. (1)–(4) leads to:

$$n_{av} = \frac{1}{2k} \cdot \frac{0.5+d}{(2d)^2} \cdot \frac{1}{x^2} \qquad (5)$$

The value of d is obtained from the convolution integral of the phantom pattern and line spread function of the system, and is a function of the ratio of x to the system spatial resolution. The line spread function is assumed to be a normal Gaussian distribution function. Then, the system spatial resolution is represented in terms of the standard deviation σ_t, or full width at half maximum (FWHM) R_t ($=2.35\sigma_t$).

Experiments were carried out to determine the k value. Several bar phantoms were observed with various information densities by the use of a high-resolution detector and ^{57}Co source (122ke V). Bar phantoms were placed just before the detector without collimators. Other experimental procedures were analogous to the main experiments, which will be described later. The results are shown in Fig. 2. The value of k and σ_t were determined by the least-square method as $\sigma_t = 1.5$ mm and $k = 0.172$. The curve which corresponds to eq. (5) is also shown in the same figure.

Scinti-photo Resolution Versus Product of Radioactivity and Imaging Time

The whole field viewed by the system is assumed to be totally covered with a bar phantom. Then,

$$n_{av} = N/S_d \qquad (6)$$

where N is the total count in the scintigram, and S_d the area of the field of view. Since the total count is related to the product of total activity and imaging time:

$$\frac{N}{AT} = \frac{n_{av}}{aT} = 1.11 \cdot 10^9 \eta \cdot e_w \cdot e_p \cdot g \quad (\text{cts} \cdot \text{min.}^{-1} \cdot \text{mCi}^{-1}) \qquad (7)$$

where A is the total activity of the flood source which is as large as the field of view of the detector (mCi); a, activity density ($= A/S_d$) (mCi/cm^2); T,

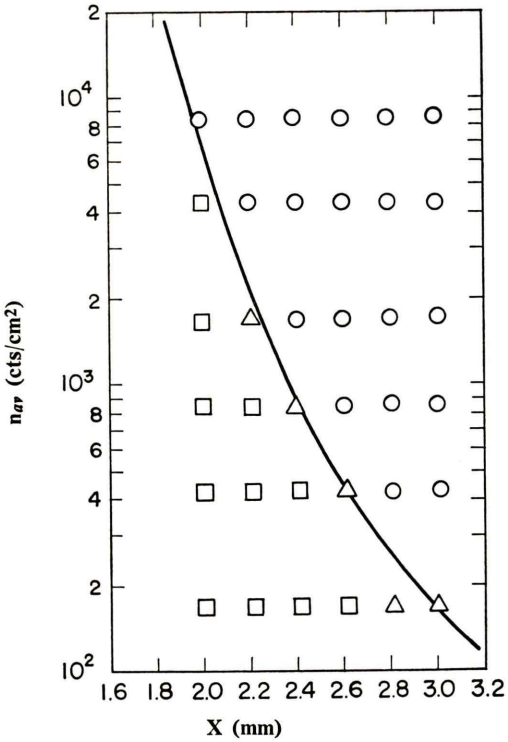

Fig. 2 Scinti-photo classification and adaption of eq. (5) to obtain k value.

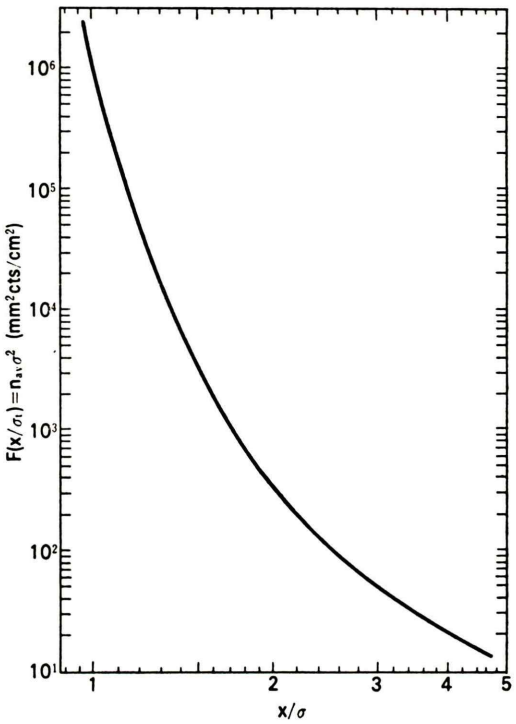

Fig. 3 Relation between x/σ_t and F (x/σ_t).

imaging time (min); η, number of emitted gamma-rays per disintegration; g, efficiency of the collimator; e_p, the photopeak efficiency of the scintillator; and e_w, efficiency of the pulse-height selector (i.e. the ratio of the number of pulses impinging in the window of the pulse-height selector to that involved in the photopeak).

Equation (5) is rewritten as:

$$n_{av}\cdot\sigma_t^2 = \frac{1}{2k}\cdot\frac{0.5+d}{(2d)^2}\cdot\frac{1}{(x/\sigma_t)^2} = F(x/\sigma_t). \quad (8)$$

Therefore, the term $n_{av}\cdot\sigma_t^2$ is only a function of x/σ_t, because d is also a function of x/σ_t as described before. The following equation is derived from eqs. (7) and (8):

$$aT = 9.01\cdot10^{-10}\cdot\frac{F(x/\sigma_t)}{\sigma_t^2\cdot n\cdot e_w\cdot e_p\cdot g} \quad (9)$$

In this equation, the efficiency of bar phantoms (i.e. the ratio of the number of gamma-rays passing through the phantom to that coming in) is assumed to be 0.5. The minimum product of activity density and imaging time (to be denoted as critical aT) for resolving the distance x is determined by this equation. The relation between x/σ_t and $F(x/\sigma_t)$ is shown in Fig. 3.

Optimum Collimators

Parallel-hole collimators were investigated by Anger[6,7]. When his analysis is applied, g_o, the largest efficiency of a collimator among collimators having a certain resolution R_c(FWHM) is expressed as follows:

$$g_o = \left(\frac{KR_c}{2m\mu^{-1}}\right)^2\left(\frac{1}{\sqrt{\lambda}+1}\right)^4 \quad (10)$$

$$\lambda = \frac{b+c}{2m\mu^{-1}} \quad (11)$$

where

K=a constant equal to 0.282[6,7],

m=a constant equal to 5[8],
μ^{-1}=the mean free path of gamma-rays in the collimator septal material,
b=the distance from a radioactive subject to the entrance of the collimator,
c=the distance from the middle plane of the scintillator to the exit of the collimator.

Such collimators having g_o (shown in eq. (10)) are always considered hereafter unless a certain collimator is specifically designated.

Selection of Collimator

The relation between the critical aT and x was calculated under the conditions in which a collimator for use with ^{99m}Tc was attached to the detector. A bar phantom and ^{99m}Tc flood source were assumed to be 100 mm away from the collimator surface. Calculations were done with several different collimators. The value of R_t is taken as $(R_c^2+R_i^2)^{1/2}$, where R_i is the resolution of the detector in terms of FWHM (i.e. $R_i=2.35\cdot\sigma_i$). Other conditions are: $\eta=1.0$, $e_w=1.0$, $e_p=0.707$ (for 9.0 mm thick NaI(Tl) crystal), and $\sigma_i=1.5$ mm. The results obtained with three typical collimators are shown in Fig. 4.

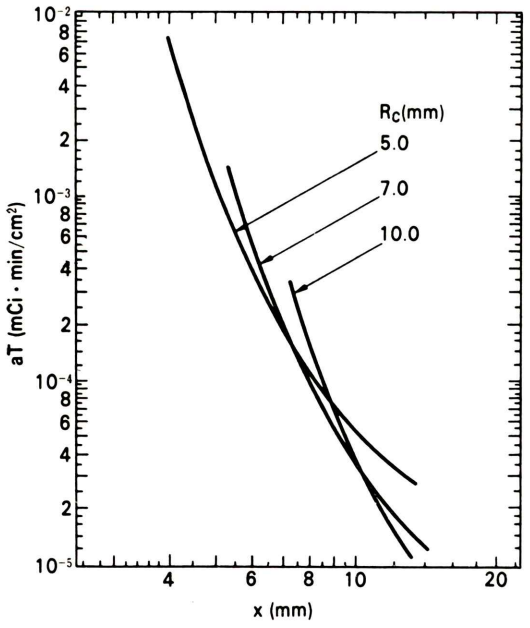

Fig. 4 Selection of collimators. Critical aT versus x is shown for three systems, each of which consists of the same detector and different collimator.

Under the conditions of $aT=3\cdot10^{-4}$(mCi·min/cm^2) (i.e. $A=10$ mCi when $S_d=1{,}000$ cm^2, and $T=0.03$ min), for example, the values of x obtained from the intersections with the curves $R_c=5$, 7 and 10 mm are 6.2, 6.5 and 7.4 mm respectively. In this case, the best resolution was achieved with the collimator having $R_c=5$ mm. On the other hand, the collimator with $R_c=7$ mm was the best in case $x=8$ mm was to be resolved, because the latter provided the minimum aT value among these three collimators in resolving $x=8$ mm.

The relation between aT and x thus represents the performance characteristics inherent to a scintillation camera system. The authors call the curve showing this relation "the characteristic curve of the system". The characteristic curves enable us to select the optimum collimator when the performance of a scintillation camera and imaging conditions are given.

Evaluation of Scintillation Camera

Assuming that the collimator optimum to any value of aT is available, the relation between aT and x represents the characteristic curve inherent to a scintillation camera detector. This curve corresponds to the envelope of the characteristic curves, each of which characterizes a system consisting of a given detector with the afore-mentioned optimum collimator. The characteristic curves thus obtained are shown in Fig. 5 for scintillation cameras having various R_i values.

Fig. 5 shows that the smaller value of R_i a system has, the better performance the system can achieve (i.e. a better system can take a smaller value of aT for a certain fixed value of x, and vice versa).

Fig. 5 also shows that the increment in the system performance, caused by the decrease in the value of R_i, lessens as R_i takes smaller values or x takes larger values, that is, changing the system from one having $R_i=5.42$ mm to another with $R_i=3.53$ mm lowers the critical aT required for visualizing 4 mm of x down to about one fifth but for 6 mm of x only to a half. In other words, an

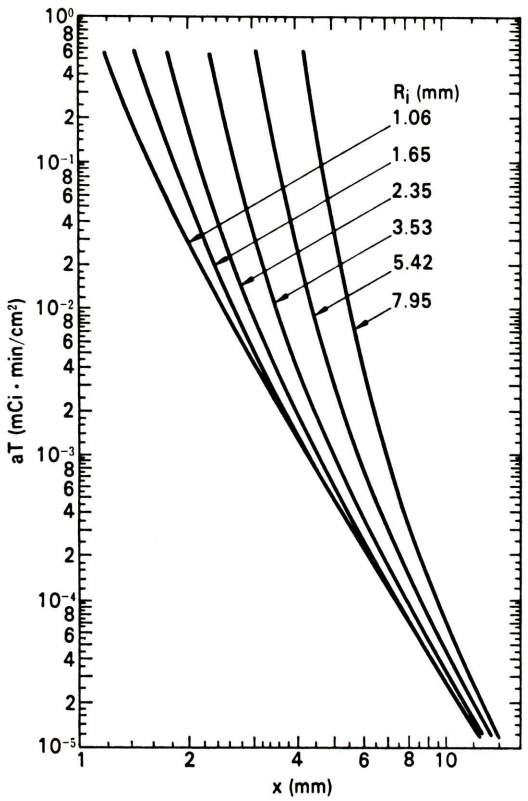

Fig. 5 Evaluation of detectors. Critical aT versus x is shown for six detectors with optimum collimators according to aT values.

improvement in R_i becomes less effective as the value of R_i decreases or x increases.

Experimental Evaluation of Four Systems

Characteristic curves were experimentally obtained with four different scintillation camera systems which are all commercially available, and were compared with culculated results. Several parameters of each system are shown in Table 1. Scintillation crystal thickness of System A developed by authors[9], is 9 mm, and those of the other systems are all 12.7 mm.

Low-energy, high-resolution collimators were selected from among the standard collimators of each system. Only with System B, the "All Purpose Collimator" was used since only this collimator was available for our experiments. Bar phantoms

Table 1 Resolution and efficiency of systems

System	R_t* (mm)	R_i** (mm)	R_c** (mm)	$e_p g$*
A	6.6	3.7	5.5	$4.58 \cdot 10^{-5}$
B	12.2	5.5	11	$19.7 \cdot 10^{-5}$
C	11.2	6.5	9	$12.5 \cdot 10^{-5}$
D	8.1	5.4	6	$6.68 \cdot 10^{-5}$

* Measured.
** Cited from catalog, or estimated.
R_t: System-resolution (FWHM) for ^{99m}Tc gamma-rays
R_i: Detector-resolution (FWHM) for ^{99m}Tc gamma-rays
R_c: Collimator-resolution (FWHM) at 100 mm from collimator surface
e_p: Photopeak-efficiency for ^{99m}Tc gamma-rays
g: Collimator-efficiency

were placed 100 mm away from the collimator surfaces. Flood sources of ^{99m}Tc were placed just behind bar phantoms. The source activities were in the range of 0.007–0.005 mCi/cm² for all the measurements. The selected information densities were in the range of about 15–0.05 kcts/cm², being varied approximately by a factor of 2. All the scinti-photos were exposed on Polaroid Type 107 films. Image sizes were adjusted in such way that the entire field of view of a system covers a circular area having about 70 mm diameter of each film. All the bar phantom scinti-photos were classified by human eye measurements into the following three classes: resolved, critical, and unresolved. Scinti-photos resolving two adjacent bars over 70–80 percent of the total areas were classified as "critical". Those with larger resolved areas were classified as "resolved" and those with smaller resolved areas as "unresolved". Results of the classification were not virtually affected by the scatter in film density due to limited time for exposure adjustments. Several scintigrams were taken also on 11″×14″ X-ray films with a small-dotted imaging device, and what interested the authors was that the classification with these films showed the same results as with Polaroid films.

The window width of the pulse-height selector was maintained at 20% through all the experiments. The corresponding e_w were determined experimentally. The aT values at $e_w=1.0$ were then calculated to compare the system sensitivities.

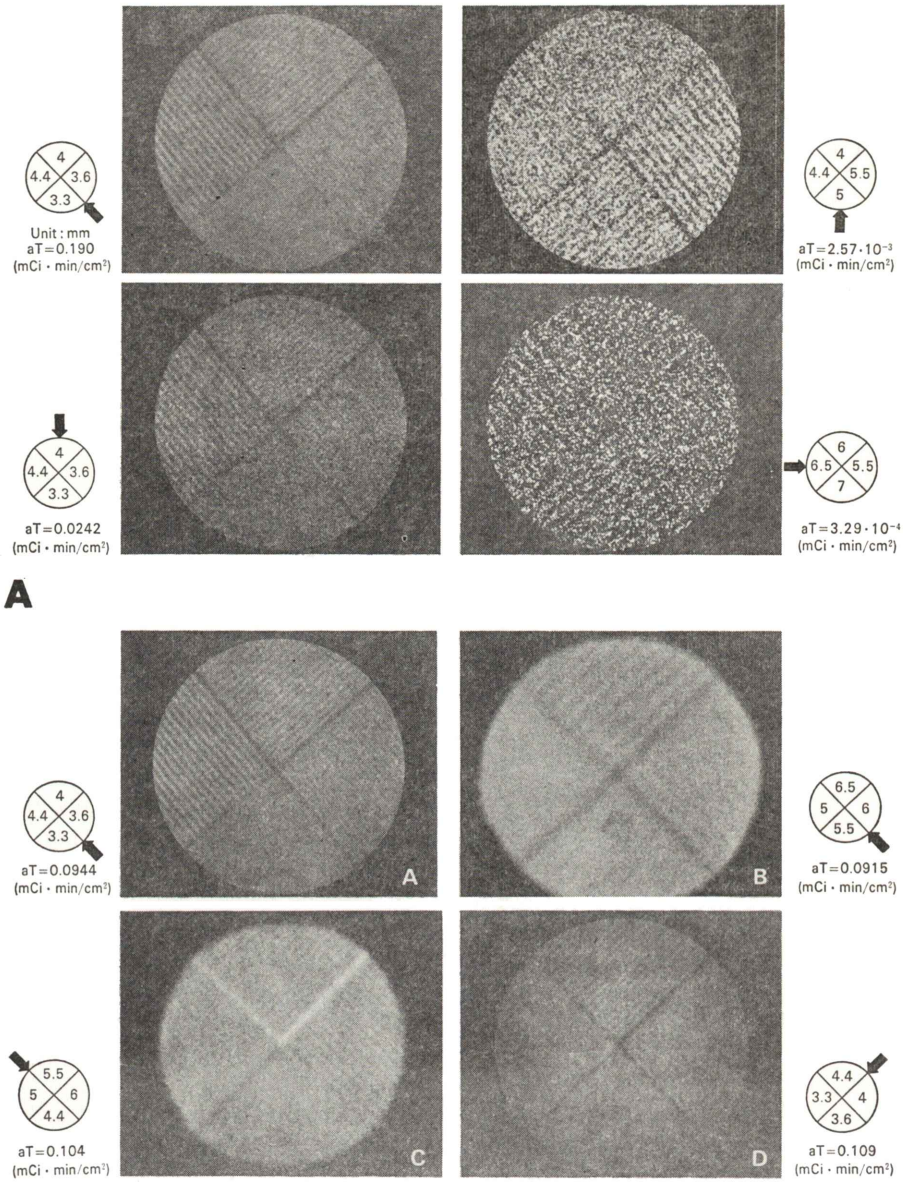

Fig. 6 Examples of scinti-photos. They show images of bar phantoms placed 100 mm away from the collimator surfaces. The numbers in circles are bar width of the corresponding positions in the scinti-photos. The arrows outside the circles show the critical bar width for individual conditions.

(A) Scinti-photos taken with System A with various values of aT.

(B) Scinti-photos with Systems A, B, C, and D with approximately the same values of aT.

Some examples of scinti-photos are shown in Fig. 6. The results of scinti-photo classification with System A are shown in Fig 7. The value $\eta \cdot e_p \cdot g$ was $4.02 \cdot 10^{-5}$ obtained from the experimental values of a, T, and n_{av} by the use of eq. (7). The value σ_t was 2.8 mm obtained from the line spread function measurement. The characteristic curve of this system calculated from eq. (9) is shown as the broken line in Fig. 6. This curve should pass through the critical points in the figure. Meanwhile, the solid line which corresponds to $\eta \cdot e_p \cdot g = 4.58 \cdot 10^{-5}$ appears to agree better with these points. The difference between the two $\eta \cdot e_p \cdot g$ values, however, rests within the range of experimental errors. Therefore, the calculation based on eq. (9) is enough accurate over the relatively wide range under consideration. The

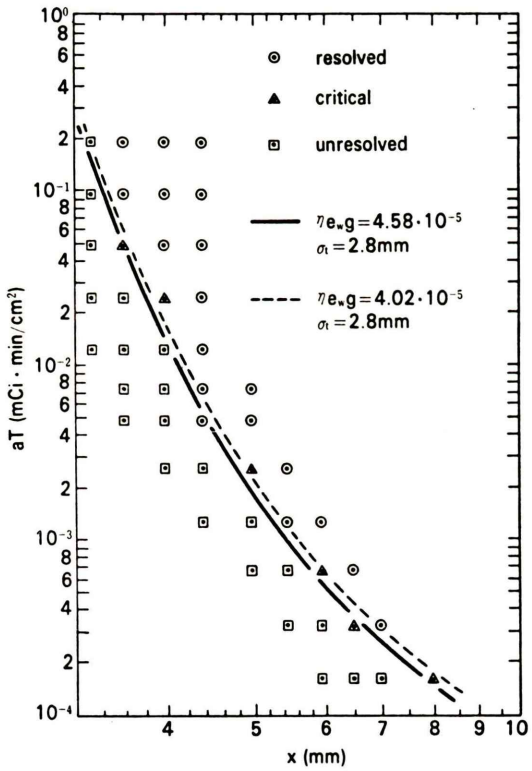

Fig. 7 Scinti-photo classification and characteristic curves of System A. Curves shown in broken and solid lines were calculated with parameters experimentally obtained and with ones modulated within the range of experimental errors, respectively.

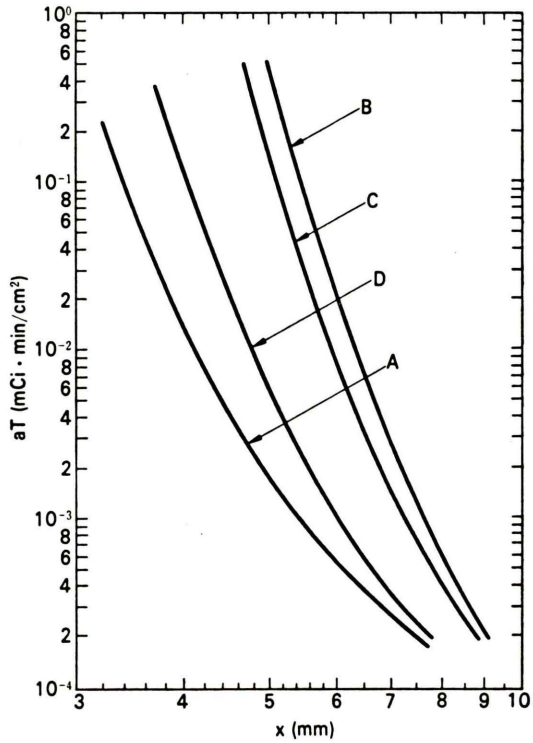

Fig. 8 Evaluation of four systems. Performance of each System A, B, C and D is shown with the characteristic curve.

agreements in the other three systems are as good as in System A.

The four characteristic curves thus obtained are shown in Fig. 8. The performance comparison among the four systems made from this figure reveals that System A is the best and Systems D, C and B follow in that order.

Scintillation crystal thickness is the primary determining factor of e_p. The change in the thickness from 12.7 to 9.0 mm decreases the values of e_p by 6 percent and 23 percent for ^{99m}Tc and ^{131}I gamma rays respectively, and increases the critical value of aT by the same factors. However, resolution of detector also has a significant effect on critical aT as shown in Fig. 5. In fact, System A being equipped with a 9 mm thick scintillation crystal provided the least value of aT in comparison with the other three systems each having a 12.7 mm thick scintillation crystal as shown in Fig. 8.

Conclusion

The theoretical analysis on scintigram resolution introduces a method of evaluation of scintillation camera system. This method, in which the theoretical results agree well with experimental results, is based on observation of bar phantom images with human eyes.

Images showing distribution of radioisotope locally concentrated in clinical object may be simulated by bar phantom images, so that the results of this article may be applied, for example, to case of bone scanning. Further investigation, however, will be required to clarify the difference between visibility of bar patterns and unknown patterns such as spherical tumors.

For the case of diffuse distribution of radioisotopes such as liver scanning, system performance may be estimated from modification of the present analysis, which will be reported in a separate paper.

Acknowledgment

The authors are indebted to Dr. Fumio Kinoshita of Ohkubo Municipal Hospital, Dept. of Radiology, Dr. Toshiro Yamasaki of Tokyo Women's Medical College, Dr. Yoshihiro Inoue of Mitsui Memorial Hospital, Dept. of Radiology, Dr. Katsumi Takami, and Mr. Fumio Kawaguchi of Hitachi Central Research Laboratory, for their valuable discussions and technical suggestions.

The present work was originally presented at the 273th Kanto District Meeting of Japan Radiological Society in February 1976, and then at the 16th Annual Meeting of Japanese Society of Nuclear Medicine in November 1976.

REFERENCES

1) Coltman JW: Scintillation limitations to resolving power in imaging devices. J Opt Soc Am **44**: 234–237, 1954
2) Iinuma T and Fukuhisa K: Digital simulation of radioisotope imaging (1). On the recognition of a defect in plane source by human observer. Nippon Acta Radiologica **31**: 1270–1285, 1972 (In Japanese)
3) Rollo FD and Schulz AG: A contrast efficiency function for quantitatively measuring the spatial-resolution characteristics of scanning systems. J Nucl Med **11**: 53–60, 1970
4) Rollo FD: An index to compare the performance of scintigraphic imaging systems. J Nucl Med **15**: 757–762, 1974
5) Keller EL and Coltman JW: Modulation transfer and scintillation limitations in gamma-ray imaging. J Nucl Med **9**: 537–545, 1968
6) Anger HO: Scintillation camera with multichannel collimators. J Nucl Med **5**: 515–531, 1964
7) Anger HO: Instrumentation in Nuclear Medicine, Vol. 1, Hine GJ, ed. Academic Press, New York, 1967, p. 520
8) Pamela M and Kibby BA: The design of multichannel collimators for radioisotope cameras. Brit J Radiol **42**: 91–101, 1969
9) Nagasawa Y, Ishimatsu K, and Tabuchi H: Development of a scintillation camera "GAMMA VIEW." Hitachi Hyoron **59**: 168–172, 1977 (In Japanese) and abstract in Hitachi Review **26**: 102, 1977

要 旨

シンチフォトの分解能とシンチカメラシステムの評価

石松健二*, 植田 健**, 田中正敏*, 向井信之*

* ㈱日立メディコ, ** ㈱日立製作所中央研究所

シンチレーションカメラシステムで得られるシンチグラムの解像度は, 装置自体の解像度と感度以外に, RI投与量 (a) と撮影時間 (T) が関与する. すなわち, 上記 a と T の積とシンチグラムの解像度との関係を表わす特性曲線は, 検出器およびコリメータの感度と解像度によって決定される. この特性曲線を理論的に検討し, 特性曲線が使用条件に応じたコリメータの選択やカメラの評価に利用できることを示した.

次に, 4機種のシンチレーションカメラシステムについて, バーファントム解像度を実験的に評価した. 実験データによる特性曲線は, 計算結果と実験誤差の範囲内で一致した.

低エネルギー核種では, 装置の感度の改善よりも解像度の改善の方がシンチグラムの向上に大きく寄与することが結論された.

Key word: Scintigram resolution